Astrocytes potentiate GABAergic transmission in the thalamic reticular nucleus via endozepine signaling

Catherine A. Christian[1] and John R. Huguenard

Department of Neurology and Neurological Sciences, Stanford University, Stanford, CA 94305

Edited by Ben A. Barres, Stanford University, Stanford, CA, and approved October 23, 2013 (received for review September 24, 2013)

Emerging evidence indicates that diazepam-binding inhibitor (DBI) mediates an endogenous benzodiazepine-mimicking (endozepine) effect on synaptic inhibition in the thalamic reticular nucleus (nRT). Here we demonstrate that DBI peptide colocalizes with both astrocytic and neuronal markers in mouse nRT, and investigate the role of astrocytic function in endozepine modulation in this nucleus by testing the effects of the gliotoxin fluorocitrate (FC) on synaptic inhibition and endozepine signaling in the nRT using patch-clamp recordings. FC treatment reduced the effective inhibitory charge of $GABA_A$ receptor ($GABA_AR$)-mediated spontaneous inhibitory postsynaptic currents in WT mice, indicating that astrocytes enhance $GABA_AR$ responses in the nRT. This effect was abolished by both a point mutation that inhibits classical benzodiazepine binding to $GABA_ARs$ containing the α3 subunit (predominant in the nRT) and a chromosomal deletion that removes the *Dbi* gene. Thus, astrocytes are required for positive allosteric modulation via the α3 subunit benzodiazepine-binding site by DBI peptide family endozepines. Outside-out sniffer patches pulled from neurons in the adjacent ventrobasal nucleus, which does not contain endozepines, show a potentiated response to laser photostimulation of caged GABA when placed in the nRT. FC treatment blocked the nRT-dependent potentiation of this response, as did the benzodiazepine site antagonist flumazenil. When sniffer patches were placed in the ventrobasal nucleus, however, subsequent treatment with FC led to potentiation of the uncaged GABA response, suggesting nucleus-specific roles for thalamic astrocytes in regulating inhibition. Taken together, these results suggest that astrocytes are required for endozepine actions in the nRT, and as such can be positive modulators of synaptic inhibition.

thalamus | glia | uncaging | electrophysiology | epilepsy

Benzodiazepines are widely used in the treatment of neurologic disorders, such as epilepsy, anxiety, and sleep disturbances. The classical mode of benzodiazepine action is allosteric potentiation of ionotropic currents through type A receptors for the inhibitory neurotransmitter GABA benzodiazepine-binding sites on $GABA_A$ receptors ($GABA_ARs$) (1). The identification of benzodiazepine-binding sites in the CNS (2, 3) led to the hypothesis that endogenous brain-derived benzodiazepine-mimicking substances (i.e., endozepines) may exist (4). The 10-kDa peptide diazepam-binding inhibitor (DBI) and associated cleavage products bind to $GABA_AR$ benzodiazepine-binding sites (5–7), but physiological roles for such substances are not well defined.

DBI mRNA transcript and peptide immunoreactivity have been observed in various brain regions in both neurons (8) and glial cells (9–12). DBI-derived peptides, including triakontatetraneuropeptide (34 amino acids), octadecaneuropeptide (18 amino acids), and octapeptide (8 amino acids), are secreted by astrocytes (13–18). The release of endozepines by cultured glial cells can be inhibited by GABA or somatostatin (14, 15) and stimulated by beta-amyloid peptide or pituitary adenylate cyclase-activating polypeptide (16–18). DBI peptides also have been demonstrated to affect astrocytic function via actions on the mitochondrial benzodiazepine receptor, also known as 18-kDa translocator protein, which influences GABA receptor activation through modulation of neurosteroid production (19, 20). Endogenous regulation of endozepine actions by native glial cells and subsequent effects on synaptic inhibition remain to be demonstrated.

The thalamic reticular nucleus (nRT) is a brain structure in which endozepines regulate synaptic inhibition and suppress absence seizure activity (21). The nRT acts as an anatomical and functional gate between the thalamus and cortex, receiving excitatory inputs from corticothalamic and thalamocortical axons and powerfully inhibiting thalamocortical relay cells in the dorsal thalamus (22, 23). Intra-nRT inhibition arises from recurrent collateral connections between nRT cells, and modulation of intra-nRT inhibition can bidirectionally regulate the thalamic oscillatory activity that is a hallmark of absence seizures. Specifically, reductions in intra-nRT inhibition drive hypersynchronous epileptiform oscillations between the nRT and the adjacent ventrobasal nucleus (VB) (24), whereas gains in intra-nRT inhibitory strength suppress epileptiform oscillatory duration and power (25).

Our recent work suggests that DBI-derived endozepines in the nRT act in the latter mode, by potentiating inhibitory $GABA_AR$-mediated currents (21). These endozepine actions are absent in α3(H126R) mutant mice, in which classical benzodiazepine binding via α3-containing $GABA_ARs$ is abolished, and in *nm1054* mutant mice, which lack the *Dbi* gene (21, 26, 27). Which cells in the nRT (glia, neurons, or both) are primarily involved in nRT endozepine actions remains unclear.

Here we tested the effects of fluorocitrate (FC), a glia-selective metabolism inhibitor that blocks the aconitase enzyme, which has been shown to be effective in reducing astrocytic function both in vivo and in vitro (28–30), on synaptic inhibition and allosteric modulation of GABAergic currents in the thalamus. Our findings indicate that astrocytes are required for modulation of synaptic inhibition by DBI-derived endozepines in the nRT.

Significance

Benzodiazepines are commonly prescribed to treat neuropsychiatric disorders, and produce clinical effects on sleep, anxiety, and seizures by augmenting synaptic inhibitory currents through $GABA_A$ receptors. Our previous work has indicated that peptides of the diazepam-binding inhibitor family act as endogenous benzodiazepines (endozepines) in the thalamic reticular nucleus (nRT), where they mediate antiepileptic and other effects. Here we report that astrocytes are required for the actions of endozepines on GABAergic transmission in the nRT. Thus, astrocytes in nRT are specialized to contribute to a localized increase in efficacy of synaptic inhibition relevant to endogenous seizure control.

Author contributions: C.A.C. and J.R.H. designed research; C.A.C. performed research; C.A.C. analyzed data; and C.A.C. and J.R.H. wrote the paper.

The authors declare no conflict of interest.

This article is a PNAS Direct Submission.

[1]To whom correspondence should be addressed. E-mail: cchristian@stanford.edu.

This article contains supporting information online at www.pnas.org/lookup/suppl/doi:10.1073/pnas.1318031110/-/DCSupplemental.

Results

DBI Peptide is Expressed in Both Astrocytes and Neurons in Mouse nRT. DBI peptide is widely expressed in the mouse thalamus (21), and previous studies have shown that DBI or its processing products are expressed in the nRT in rats (31). To examine the cellular localization of DBI peptide in mouse nRT, we used double-labeled fluorescent immunohistochemistry for DBI and either the astrocytic marker GFAP or the neuronal marker NeuN, which confirmed the presence of DBI peptide in both astrocytes and neurons in the nRT (Fig. S1). In our experiments, we focused on elucidating the astrocytic contribution to endozepine signaling in the nRT.

FC Selectively Impairs Astrocytic Function in the nRT. We investigated the glial contribution to endozepine signaling in the nRT using the gliotoxin FC (28, 29). The glia-selective impairment in the nRT induced by FC treatment was confirmed using sulforhodamine 101 (SR101), a red fluorescent dye that is selectively taken up by astrocytes (32, 33). FC treatment (100 μM for 30 min) reduced the capacity of astrocytes to incorporate the SR101 dye (Fig. 1*A*), but did not affect GFAP immunoreactivity (Fig. 1*B*). Thus, it appears that FC treatment selectively alters the functional capacity of astrocytes in the nRT while astrocytic marker expression is maintained.

The intrinsic membrane properties and cellular excitability of nRT neurons, as assessed by voltage–current (V–I) analysis in current-clamp recordings, were not altered by FC treatment (Table S1). Cell membrane capacitance, recorded in the voltage-clamp configuration, also was unaffected (control, 55.90 ± 4.47 pF, $n = 11$ cells; FC, 51.96 ± 4.70 pF, $n = 10$ cells; $P > 0.5$). Thus, the functional effects of FC in the nRT appear to be selective for astrocytes.

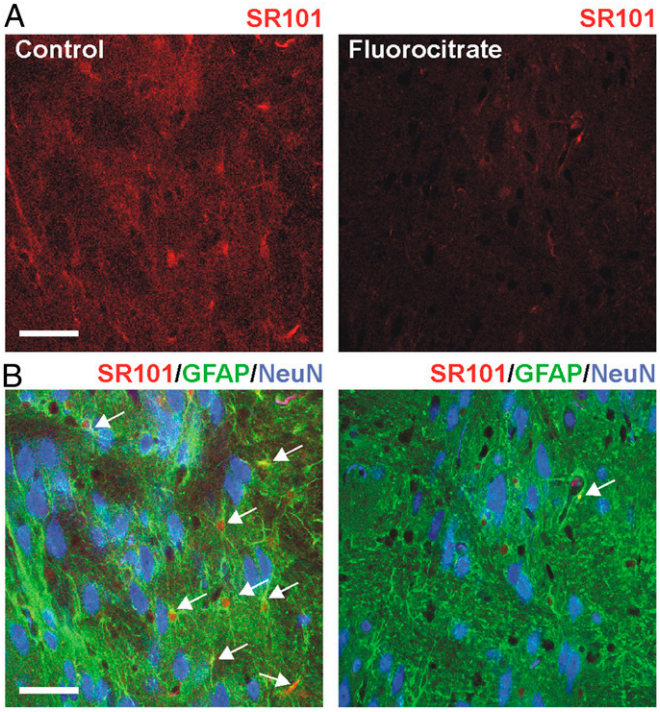

Fig. 1. Fluorocitrate selectively alters astrocytic function in the nRT. (*A*) Fluorescence images illustrating uptake of the SR101 dye in the nRT in control slices (*Left*) and after FC treatment (*Right*). (*B*) Merged image of SR101 staining (red) with immunolabeling of GFAP (green) and NeuN (blue) showing colocalization of SR101 and GFAP (yellow, arrows) in the same slices depicted in *A*. (Scale bars: 40 μm.)

Impairment of Astrocytic Function Decreases Spontaneous Inhibitory Postsynaptic Current Duration in WT nRT, an Effect Blocked by both α3(H126R) and nm1054 Mutations. If nRT astrocytes are required for endozepines to augment synaptic GABA responses, then the gliotoxin FC should decrease inhibitory postsynaptic current (IPSC) duration in the nRT. We recorded spontaneous IPSCs (sIPSCs) to test this hypothesis. In slices from WT C57BL/6 mice, FC-treated cells ($n = 22$) exhibited a decreased sIPSC duration ($P < 0.001$) compared with control cells ($n = 13$) (Fig. 2 *A*, *B*, *D*, and *E*). FC treatment did not affect sIPSC amplitude ($P > 0.15$), but did reduce sIPSC frequency (control, 2.14 ± 0.13 Hz; FC, 1.70 ± 0.13 Hz; $P < 0.05$) (Fig. 2 *F*–*G*), suggesting that presynaptic mechanisms also contribute to the effects of FC. The changes in sIPSC duration were absent in slices from α3(H126R) mice (control, $n = 12$ cells; FC-treated, $n = 10$ cells; $P > 0.3$) (Fig. 2 *C*–*E*), but the FC-induced reduction in sIPSC frequency was maintained (control, 2.02 ± 0.24 Hz; FC, 1.33 ± 0.19 Hz; $P < 0.05$) (Fig. 2*G*), indicating that presynaptic effects of FC are endozepine-independent. There were no differences in input (R_{in}, F = 0.86, $P > 0.4$) or series resistance (R_s, F = 0.24, $P > 0.8$) across these groups, demonstrating that these differences are not related to variations in recording quality. These experiments suggest that astrocytes are required for positive allosteric modulation of neuronal $GABA_A$Rs in the nRT, and that these modulators are likely endozepines that act via the α3 subunit benzodiazepine-binding site.

To determine whether FC alters nRT sIPSC duration by preventing the actions of DBI-derived peptides, we examined the effect of FC treatment in slices from *nm1054* homozygous mutants, in which the *Dbi* gene is deleted (25), and from WT littermates on the 129S6/SvEvTac background. Staining for DBI, GFAP, and NeuN demonstrated a lack of DBI colocalization in either neurons or astrocytes in *nm1054* mutant nRT (Fig. S1). As seen in C57BL/6 mice [WT strain for the α3(H126R) mutants], FC treatment resulted in decreased sIPSC duration in nRT neurons from *nm1054*-related WT mice (control, $n = 11$ cells; FC-treated, $n = 10$ cells; $P < 0.05$) (Fig. 3 *A*, *C*, and *D*); however, in *nm1054* mutants, FC had no effect on sIPSC duration (control, $n = 10$ cells; FC-treated, $n = 11$ cells; $P > 0.4$) (Fig. 3 *B*–*D*). There were no between-group differences in R_{in} (F = 0.67, $P > 0.5$) or R_s (F = 1.6, $P > 0.2$). Thus, the FC-induced reduction in sIPSC duration reflects the removal of a source of DBI-derived endozepine peptides.

FC Alters IPSC Duration in VB Neurons through Impairment of Astrocytic GABA Transporter Function. Our previous results indicate that endozepines are released in the nRT, but not in the VB (19). To examine whether the effects of FC are similarly nucleus-specific, we recorded sIPSCs in VB neurons under control conditions ($n = 14$) and after FC treatment ($n = 8$) (Fig. S2 *A* and *B*). FC treatment shifted the probability distribution for sIPSC half-width toward longer events (Fig. S2*C*, $P < 0.001$), but neither sIPSC amplitude nor sIPSC frequency were affected ($P > 0.8$), suggesting that the effects of FC in VB neurons are mainly postsynaptic.

We hypothesized that impairment of GABA uptake by astrocytic GABA transporters (GATs) (34–36) may underlie the difference in sIPSC duration. We thus tested the combined effects of the GAT-1 antagonist 1,2,5,6-tetrahydro-1-[2-[[(diphenylmethylene) amino]oxy]ethyl]-3-pyridinecarboxylic acid hydrochloride (NNC-711; 4 μM) and the GAT-3 antagonist 1-[2-[*Tris*(4-methoxyphenyl) methoxy]ethyl]-(*S*)-3-piperidinecarboxylic acid (SNAP-5114; 10 μM). These two GAT subtypes, the primary GATs expressed in the thalamus, appear to be expressed exclusively on astrocytes (37, 38). Consistent with this hypothesis, GAT antagonists increased sIPSC duration under control (i.e., intact glial function) conditions ($n = 11$; $P < 0.001$) (Fig. S2 *B* and *C*), in a manner not different from that seen after FC treatment ($P > 0.2$). There were no differences in either R_{in} (F = 0.28, $P > 0.7$) or R_s (F = 1.49, $P > 0.2$) across groups. These results suggest that, in contrast to the

NEUROSCIENCE

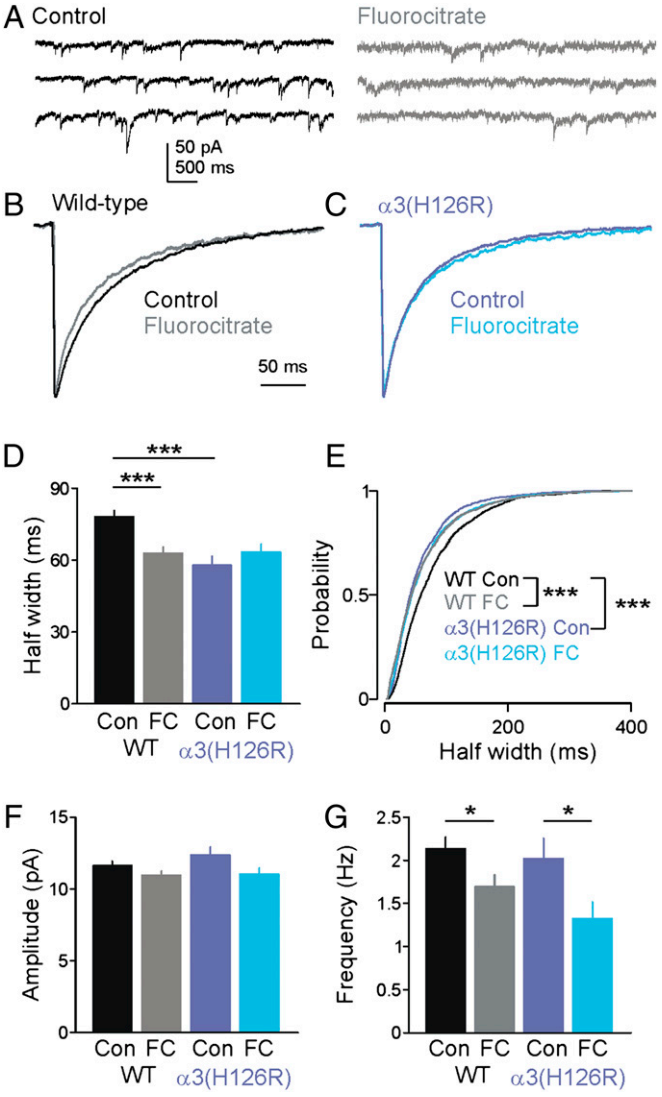

Fig. 2. Fluorocitrate reduces sIPSC duration in the nRT, and this effect is blocked by the α3(H126R) mutation. (*A*) Representative continuous traces of sIPSCs recorded in nRT cells from WT C57BL/6 mice in control conditions (*Left*) and after FC treatment (*Right*). (*B*) Averaged sIPSCs from nRT cells from WT mice in control conditions (black trace) and after FC treatment (gray trace), normalized to peak amplitude. (*C*) Averaged sIPSCs from nRT cells from α3(H126R) mice in control conditions (dark-blue trace) and after FC treatment (light-blue trace), normalized to peak amplitude. (*D*) Mean ± SEM for sIPSC half-width in WT and α3(H126R) mice. (*E*) Probability distributions comparing sIPSC half-width in WT and α3(H126R) mice in control and FC-treated conditions (n = 1,000–2,200 events/group). (*F* and *G*) Mean ± SEM for sIPSC amplitude (*F*) and frequency (*G*) in WT and α3(H126R) mice. $*P < 0.05$, $***P < 0.001$ vs. WT con (*D*, *E*, and *G*) or α3(H126R) con (*G*).

inhibition-reducing effects of FC in the nRT, GABAergic inhibition in the VB is enhanced after FC treatment, and these effects largely reflect altered GAT function.

GAT Blockade Alone Does Not Alter sIPSCs or the Response to Benzodiazepine-Binding Site Antagonism in the nRT. The opposing effects of FC on sIPSC duration in the nRT and VB could reflect differences in allosteric receptor modulation and/or differences in GAT uptake between these two nuclei. Thus, we tested the effect of GAT blockade alone on sIPSCs in the nRT. In contrast to the effects of GAT blockade in the VB, GAT blockade did not affect sIPSC duration in nRT neurons (control, n = 12; GAT blockade, n = 10; $P > 0.2$) (Fig. S3 *A* and *B*). In addition, GAT blockade did not affect the response to the benzodiazepine-binding site antagonist flumazenil (FLZ, 1 μM) (Fig. S3C), indicating that endozepine modulation of sIPSCs in the nRT remains intact when GAT function is impaired. Thus, the differing effects of FC on sIPSCs in the nRT and VB reflect nucleus-specific contributions of endozepine modulation and GAT-mediated uptake on sIPSC duration.

FC Treatment Blocks nRT Potentiation of VB Membrane Patch Responses to GABA Uncaging. We recently demonstrated that outside-out membrane "sniffer patches" pulled from VB neurons exhibit a prolonged response to focal laser photolysis of caged GABA when placed in the nRT compared with the VB (21, 39). This methodology has been termed the sniffer patch laser uncaging response (SPLURgE) (39). This effect is reduced by both benzodiazepine-binding site antagonism and the *nm1054* mutation, indicating that endozepines underlie a major part of this potentiation. To determine whether astrocyte-derived endozepines are responsible for this effect, we tested the response of sniffer patches to GABA uncaging when placed in nRT or VB of slices from C57BL/6 mice either under control conditions or after FC treatment. Under control conditions, SPLURgE duration was significantly prolonged when patches were placed in the nRT compared with the VB ($P < 0.001$; Fig. 4 and Fig. S4), confirming our previous results (21). In FC-treated slices, although an overall increase in SPLURgE duration in the VB was seen ($P < 0.05$, Fig. 4*B*), only the late decay portion of the response (i.e., the 90–10% decay time) was enhanced by placement in the nRT (half-width, $P > 0.6$; Fig. 4; 90–10% decay time, $P < 0.05$, Fig. S4).

A Combination of GAT Blockade and FLZ Mimics the Effects of Fluorocitrate on Sniffer Responses. To determine whether the increased SPLURgE duration produced by FC could be attributed

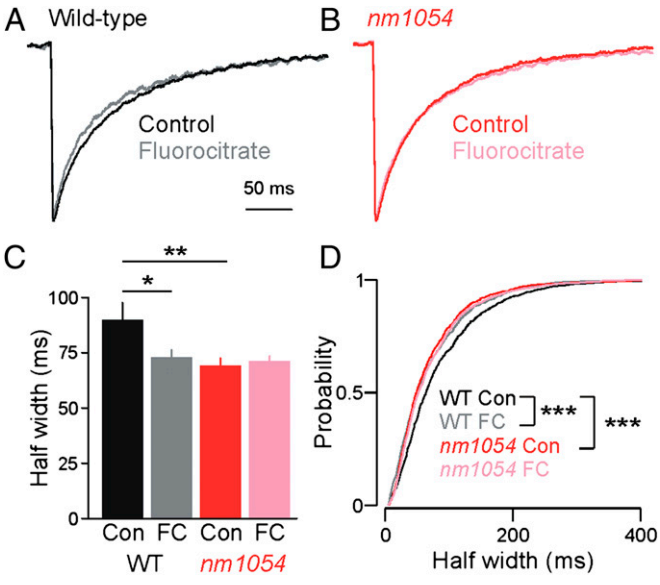

Fig. 3. Effects of fluorocitrate in the nRT are absent in *nm1054* mutant mice. (*A*) Averaged sIPSCs from nRT cells from WT littermates of *nm1054* mice in control conditions (black trace) and after FC treatment (gray trace), normalized to peak amplitude. (*B*) Averaged sIPSCs from nRT cells from *nm1054* mice in control conditions (red trace) and after FC treatment (pink trace), normalized to peak amplitude. (*C*) Mean ± SEM for sIPSC half-width in WT and *nm1054* mice. (*D*) Probability distributions comparing sIPSC half-width in WT and *nm1054* mice in control and FC-treated conditions (n = 972–1,036 events/group). $*P < 0.05$; $**P < 0.01$; $***P < 0.001$ vs. WT control (*C* and *D*).

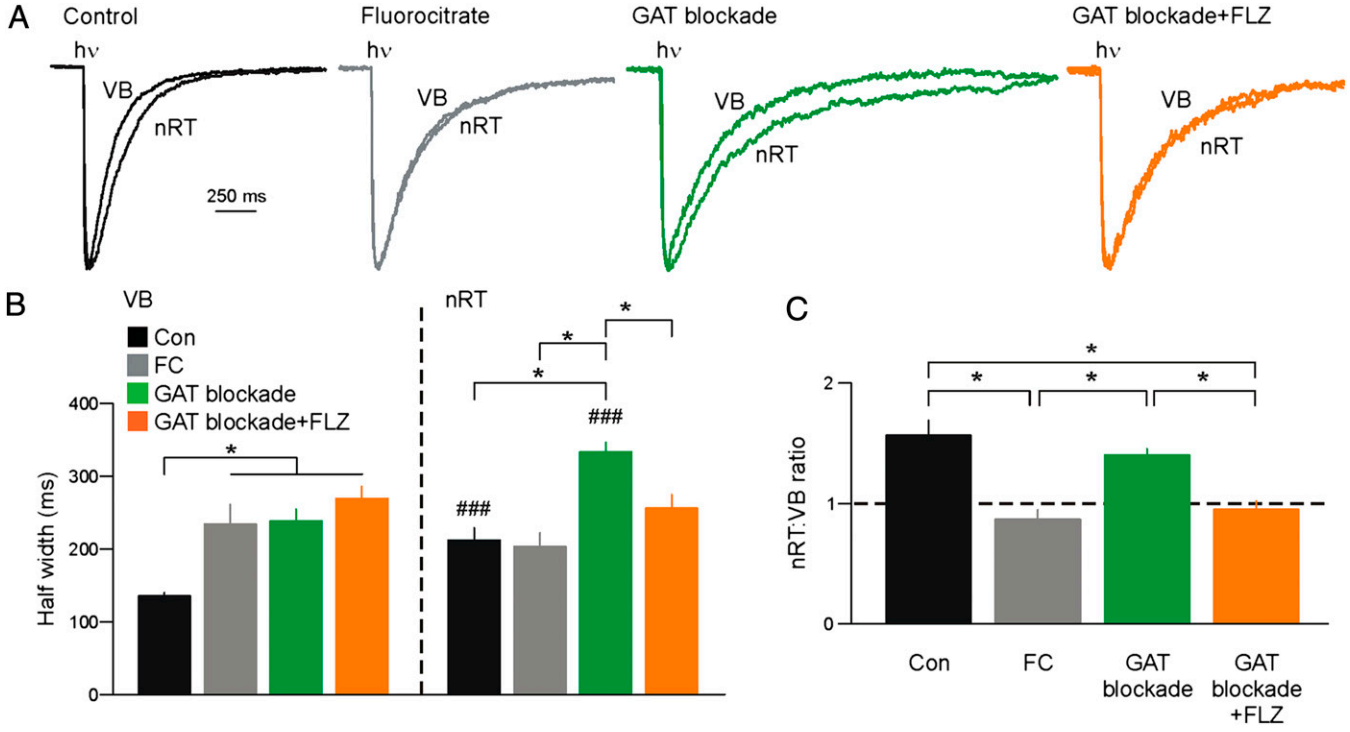

Fig. 4. Combined blockade of GATs and benzodiazepine-binding sites mimics the effects of fluorocitrate on nRT potentiation of VB membrane patch responses to GABA uncaging. (*A*) Responses to GABA uncaging averaged across all outside-out patches pulled from VB neurons and recorded after placement in either VB or the nRT in control conditions (black traces), after FC treatment (gray traces), GAT blockade (green traces) or combined GAT blockade plus FLZ (orange traces). Currents are normalized to the peak amplitude. All traces are shown to the same scale. (*B*) Mean ± SEM for half-width of uncaging responses recorded under control conditions (black bars), after FC treatment (gray bars), in the presence of GAT antagonists (green bars), or in the presence of GAT antagonists and FLZ (orange bars). Each bar represents between six and nine patches. (*C*) Mean ± SEM for ratio of values obtained when patches placed in the nRT compared with averaged value for patches placed in VB for each respective group. hν, 1-ms UV laser stimulus. $^{*}P < 0.05$; $^{\#\#\#}P < 0.001$ vs. respective group values for patches placed in VB.

to GAT disruption, we directly tested the effects of GAT blockade on the responses. GAT blockade increased the SPLURgE duration of patches placed in the VB to the same degree as that seen after FC treatment ($P < 0.05$ compared with control; Fig. 4*B* and Fig. S4*A*), suggesting that the FC-increased duration of response could be attributed entirely to astrocytic GABA transport blockade. Under these conditions, however, potentiation of the SPLURgE by placement in the nRT was preserved (difference in VB vs. nRT response, both after GAT blockade; $P < 0.001$; Fig. 4 *B* and *C* and Fig. S4) to the same degree as that in control conditions (Fig. 4*C* and Fig. S4*B*), indicating that GAT blockade does not interfere with the endozepine-dependent enhancement of the SPLURgE. Furthermore, treatment with FLZ in the presence of the GAT antagonists prevented nRT-dependent potentiation while preserving the prolongation of responses in the VB (Fig. 4 *B* and *C* and Fig. S4). In addition, similar to FC, combined GAT blockade and FLZ did not significantly affect SPLURgE half-width, but prolonged the 90–10% decay time (Fig. 4*B* and Fig. S4*A*). This result confirms and extends our previous finding in *nm1054*-related WT mice that the combination of GAT antagonists and FLZ is sufficient to block nRT-dependent potentiation of the uncaging response (21).

Taken together, these results suggest that the effects of FC on the SPLURgEs involve a combination of impaired GAT function, largely restricted to the VB, and loss of endozepine signaling in the nRT. Thus, glial mediation of endozepine action is primarily responsible for the nRT-dependent potentiation of uncaging responses.

Discussion

A growing body of evidence demonstrates that astrocytes affect and modulate neuronal function in a wide variety of ways throughout the lifespan (40). Using the gliotoxin FC to selectively impair astrocytic function, we have shown that astrocytes are required for the modulation of synaptic inhibition by DBI-derived endozepines in the nRT. These effects are lost in both α3(H126R) and *nm1054* mutant mice, which harbor deficits in benzodiazepine binding and DBI expression, respectively. We also demonstrate that astrocytic modulation of the response of thalamic $GABA_A$Rs to GABA reflects a combination of at least two effects, GABA uptake via GATs and endozepine action. These findings demonstrate a unique mechanism by which astrocytes can modulate fast synaptic inhibition, and have implications for understanding the role of neuromodulation of thalamic synaptic inhibition in the normal functions of sleep and sensory processing as well as in pathological states, such as absence seizures.

The results presented here provide further insight into the epileptogenic effects of FC. Intravenous, intracranial, or i.p. injections of the FC precursor fluoroacetate can cause spike-and-wave discharges (SWDs) and absence seizures in various species, including mice, cats, dogs, and rabbits (41–44), with varying latencies and dose dependencies. With respect to the present study, the observation that injection of fluoroacetate in cats was found to lead to paroxysmal (40 Hz) activity in the nRT shortly before the development of synchronized SWD cortical activity (41), is particularly intriguing. Our present results suggest a cellular mechanism for this effect in the nRT: a decrease in synaptic inhibition as reflected in decreased sIPSC duration, owing to a loss of

endozepine signaling, and reduced sIPSC frequency. The development of SWD activity and absence seizures as a consequence of FC treatment is thus consistent with the hypothesized role for intra-nRT inhibition in decreasing thalamocortical oscillatory circuit activity (24), although other nonendozepine actions, such as reduced glutamate uptake and recycling (45), also could contribute to seizures, as could effects of astrocytic disruption in regions outside of the thalamus.

Whereas sIPSC duration was decreased by FC treatment in WT nRT, sIPSCs in VB neurons could be enhanced, and this effect was mimicked by GAT blockade. Although the impaired GAT function as a result of FC treatment may possibly mask a loss of endozepine signaling in this nucleus, this is unlikely given our previous findings that FLZ alone does not affect VB sIPSCs (21), as well as the results of our SPLURgE experiments demonstrating that SPLURgEs obtained in the VB in the presence of GAT antagonists do not differ from those obtained after the addition of FLZ. These results thus provide further evidence that endozepines apparently are not expressed in the VB (21). Furthermore, potentiated sIPSCs in VB cells would be expected to enhance postinhibitory rebound responses in these cells (46), suggesting another mechanism that may contribute to FC-induced SWD.

The differing effects of FC and GAT blockade on synaptic inhibition in the nRT and VB suggest that the mechanisms of astrocytic modulation of GABAergic function likely vary widely across different brain areas. Although the modulation of $GABA_B$ responses via GAT activity is well established (35, 47–49), investigations into $GABA_A$R-mediated IPSCs have yielded inconsistent findings. Tonic inhibition and evoked currents appear to be more affected by GAT activity compared with spontaneous synaptic currents (34, 36, 47, 50, 51), perhaps reflecting contributions of GABA receptors at extrasynaptic locations tightly regulated by GATs (35). The results presented here, showing the apparently stronger GAT activity in the VB than in the nRT, suggest that differential GAT activity may underlie at least some of these apparent discrepancies.

In the hippocampus, astrocytes can indirectly increase synaptic inhibition by releasing glutamate, which activates ionotropic glutamate receptors on interneurons, leading to increased GABA release (52). Conversely, pathological activation of astrocytosis in the hippocampus also has been shown to decrease synaptic inhibition as a result of glutamate/glutamine cycle disruption (53), which may explain the reductions in sIPSC frequency in the nRT after FC treatment seen in the present study. Astrocytes themselves also may be a source of GABA, as demonstrated in the cerebellum, the olfactory bulb, and cultured hippocampal cells (54–56), and chelating astrocytic calcium in the barrel cortex alters the excitability of nearby neurons in a manner similar to that of combined $GABA_A$ and $GABA_B$ receptor blockade (57). As demonstrated in the present study, endozepine signaling adds to this growing list of the mechanisms by which astrocytes can modulate fast synaptic inhibition.

In contrast to the nucleus-specific effects of GAT blockade alone on sIPSCs in the nRT and VB, SPLURgE duration was increased after GAT blockade in both nuclei. This finding likely reflects the differences in methodology and $GABA_A$R populations studied in each experiment, and suggests either that GABAergic currents mediated by nRT $GABA_A$Rs are not as sensitive to GABA uptake as receptors in VB neurons, or that GABA uptake itself is less robust in the nRT than in the VB. We recently demonstrated that the 90–10% decay time SPLURgE parameter, representing the late decay kinetics of the responses, is more sensitive to changes in GAT function than the half-width, or early decay (39). This is consistent with the results presented here, in which FC did not significantly increase the SPLURgE half-width for patches placed in the nRT, but did increase the 90–10% decay time. The further enhancement of SPLURgE 90–10% decay time under GAT block + FLZ conditions compared with FC treatment may represent a small degree of uptake mediated by GATs located on neurons rather than on astrocytes in the nRT.

Our results suggest that either nRT astrocytes release DBI endozepines or that an unknown astrocytic signal is required for neuronal endozepine release or peptide cleavage. Further experiments are needed to elucidate the mechanism(s) underlying endozepine modulation in the nRT. Identifying neuronal and astrocytic sources of secreted DBI will have implications for our understanding of the mechanisms of DBI release, which are unconventional and characterized by exophagic secretion (58). Analysis of release of the DBI homolog acyl CoA-binding protein (ACBP) indicates that soluble NSF attachment protein receptor (SNARE)-dependent fusion of vesicles containing ACBP/DBI to the plasma membrane is required for secretion (59, 60). Although there is some controversy regarding astrocytic exocytosis mechanisms (61), astrocytes appear to express functional SNARE complex components (62–64). It will be interesting to determine whether SNARE-dependent exophagy underlies DBI release from astrocytes, and whether these mechanisms exhibit region-dependent specificity.

Both of the mutant mouse models used here exhibit greater SWD activity compared with their WT counterparts (21). The present study, which demonstrates a lack of astrocytic endozepine actions in these animals, suggests that the enhancement of astrocytic mechanisms related to endozepine modulation may provide a useful therapeutic avenue for epilepsy and other neurologic diseases.

Materials and Methods

WT, α3(H126R), and *nm1054* mutant mice were bred and housed as described previously (21, 26, 65). FC stocks were prepared according to published procedures (28), and acute horizontal brain slices containing the nRT and VB were prepared following established methods (66). A subset of slices was treated with 100 μM FC for at least 30 min at room temperature. For SR101 staining, slices were incubated in 1 μM SR101 in oxygenated artificial cerebrospinal fluid (ACSF) for 20 min, washed in control ACSF for at least 10 min at 34 °C, and then fixed in 4% paraformaldehyde and processed for immunocytochemistry. In sIPSC and uncaging experiments, a CsCl-based isotonic chloride intracellular pipette solution was used, and ionotropic glutamatergic currents were blocked using kynurenic acid or D-(–)-2-amino-5-phosphonovaleric acid (APV) and 6,7-dinitroquinoxaline-2,3-dione (DNQX) in the extracellular bath solution.

Current-clamp recordings were performed using a K-gluconate pipette solution in ACSF containing kynurenic acid and picrotoxin. FLZ and the GAT antagonists NNC-711 and SNAP-5114 were bath-applied as indicated. Laser photolysis of caged GABA (100 μM) was achieved via 1-ms UV laser exposure. Experimental procedures are described in detail in *SI Materials and Methods*.

ACKNOWLEDGMENTS. We thank Isabel Parada for expert assistance with histology experiments; Corinne Badgley, Anne Herbert, and Kathy Peng for help with mouse colony maintenance and genotyping; Uwe Rudolph for providing the α3(H126R) founder mice; and Lance Lee and Mark Fleming for providing the *nm1054* founder mice. This work was supported by National Institutes of Health Grants R01 NS034774 and R01 NS006477. C.A.C. was supported by National Institutes of Health Institutional Postdoctoral Training Grant T32 NS007280, an Epilepsy Foundation of America Postdoctoral Research Fellowship, and a Katharine McCormick Advanced Postdoctoral Fellowship from Stanford University School of Medicine.

1. Gavish M, Snyder SH (1980) Benzodiazepine recognition sites on GABA receptors. *Nature* 287(5783):651–652.
2. Braestrup C, Squires RF (1977) Specific benzodiazepine receptors in rat brain characterized by high-affinity (3H)diazepam binding. *Proc Natl Acad Sci USA* 74(9):3805–3809.
3. Möhler H, Okada T (1977) Benzodiazepine receptor: Demonstration in the central nervous system. *Science* 198(4319):849–851.
4. Iversen L (1977) Anti-anxiety receptors in the brain? *Nature* 266:678.
5. Guidotti A, et al. (1983) Isolation, characterization, and purification to homogeneity of an endogenous polypeptide with agonistic action on benzodiazepine receptors. *Proc Natl Acad Sci USA* 80(11):3531–3535.
6. Alho H, et al. (1985) Diazepam-binding inhibitor: A neuropeptide located in selected neuronal populations of rat brain. *Science* 229(4709):179–182.

7. Bormann J (1991) Electrophysiological characterization of diazepam binding inhibitor (DBI) on GABAA receptors. *Neuropharmacology* 30(12B):1387–1389.
8. Alho H, Bovolin P, Jenkins D, Guidotti A, Costa E (1989) Cellular and subcellular localization of an octadecaneuropeptide derived from diazepam binding inhibitor: Immunohistochemical studies in the rat brain. *J Chem Neuroanat* 2(6):301–318.
9. Vidnyánszky Z, Görcs TJ, Hámori J (1994) Diazepam binding inhibitor fragment 33-50 (octadecaneuropeptide) immunoreactivity in the cerebellar cortex is restricted to glial cells. *Glia* 10(2):132–141.
10. Malagon M, et al. (1993) Ontogeny of diazepam-binding inhibitor-related peptides (endozepines) in the rat brain. *Neuroscience* 57(3):777–786.
11. Tonon MC, Désy L, Nicolas P, Vaudry H, Pelletier G (1990) Immunocytochemical localization of the endogenous benzodiazepine ligand octadecaneuropeptide (ODN) in the rat brain. *Neuropeptides* 15(1):17–24.
12. Alho H, Harjuntausta T, Schultz R, Pelto-Huikko M, Bovolin P (1991) Immunohistochemistry of diazepam binding inhibitor (DBI) in the central nervous system and peripheral organs: Its possible role as an endogenous regulator of different types of benzodiazepine receptors. *Neuropharmacology* 30(12B):1381–1386.
13. Loomis WF, Behrens MM, Williams ME, Anjard C (2010) Pregnenolone sulfate and cortisol induce secretion of acyl-CoA–binding protein and its conversion into endozepines from astrocytes. *J Biol Chem* 285(28):21359–21365.
14. Patte C, et al. (1999) GABA inhibits endozepine release from cultured rat astrocytes. *Glia* 25(4):404–411.
15. Masmoudi O, et al. (2005) Somatostatin down-regulates the expression and release of endozepines from cultured rat astrocytes via distinct receptor subtypes. *J Neurochem* 94(3):561–571.
16. Tokay T, et al. (2008) Beta-amyloid peptide stimulates endozepine release in cultured rat astrocytes through activation of N-formyl peptide receptors. *Glia* 56(13): 1380–1389.
17. Masmoudi O, et al. (2003) Pituitary adenylate cyclase-activating polypeptide (PACAP) stimulates endozepine release from cultured rat astrocytes via a PKA-dependent mechanism. *FASEB J* 17(1):17–27.
18. Masmoudi-Kouki O, et al. (2006) PACAP stimulates biosynthesis and release of endozepines from rat astrocytes. *Ann N Y Acad Sci* 1070:411–416.
19. Papadopoulos V, Berkovich A, Krueger KE, Costa E, Guidotti A (1991) Diazepam binding inhibitor and its processing products stimulate mitochondrial steroid biosynthesis via an interaction with mitochondrial benzodiazepine receptors. *Endocrinology* 129(3):1481–1488.
20. Gandolfo P, et al. (2000) The triakontatetraneuropeptide (TTN) stimulates thymidine incorporation in rat astrocytes through peripheral-type benzodiazepine receptors. *J Neurochem* 75(2):701–707.
21. Christian CA, et al. (2013) Endogenous positive allosteric modulation of GABA(A) receptors by diazepam binding inhibitor. *Neuron* 78(6):1063–1074.
22. Jones EG (1975) Some aspects of the organization of the thalamic reticular complex. *J Comp Neurol* 162(3):285–308.
23. Houser CR, Vaughn JE, Barber RP, Roberts E (1980) GABA neurons are the major cell type of the nucleus reticularis thalami. *Brain Res* 200(2):341–354.
24. Huntsman MM, Porcello DM, Homanics GE, DeLorey TM, Huguenard JR (1999) Reciprocal inhibitory connections and network synchrony in the mammalian thalamus. *Science* 283(5401):541–543.
25. Schofield CM, Kleiman-Weiner M, Rudolph U, Huguenard JR (2009) A gain in GABAA receptor synaptic strength in thalamus reduces oscillatory activity and absence seizures. *Proc Natl Acad Sci USA* 106(18):7630–7635.
26. Löw K, et al. (2000) Molecular and neuronal substrate for the selective attenuation of anxiety. *Science* 290(5489):131–134.
27. Ohgami RS, et al. (2005) Identification of a ferrireductase required for efficient transferrin-dependent iron uptake in erythroid cells. *Nat Genet* 37(11):1264–1269.
28. Paulsen RE, Contestabile A, Villani L, Fonnum F (1987) An in vivo model for studying function of brain tissue temporarily devoid of glial cell metabolism: The use of fluorocitrate. *J Neurochem* 48(5):1377–1385.
29. Hassel B, Paulsen RE, Johnsen A, Fonnum F (1992) Selective inhibition of glial cell metabolism in vivo by fluorocitrate. *Brain Res* 576(1):120–124.
30. Nakanishi H, Kawachi A, Okada M, Fujiwara M, Yamamoto K (1996) Protective effect of MK-801 on the anoxia-aglycemia induced damage in the fluorocitrate-treated hippocampal slice of the rat. *Brain Res* 732(1-2):232–236.
31. Costa E, Guidotti A (1991) Diazepam binding inhibitor (DBI): A peptide with multiple biological actions. *Life Sci* 49(5):325–344.
32. Nimmerjahn A, Kirchhoff F, Kerr JN, Helmchen F (2004) Sulforhodamine 101 as a specific marker of astroglia in the neocortex in vivo. *Nat Methods* 1(1):31–37.
33. Kafitz KW, Meier SD, Stephan J, Rose CR (2008) Developmental profile and properties of sulforhodamine 101–labeled glial cells in acute brain slices of rat hippocampus. *J Neurosci Methods* 169(1):84–92.
34. Keros S, Hablitz JJ (2005) Subtype-specific GABA transporter antagonists synergistically modulate phasic and tonic GABAA conductances in rat neocortex. *J Neurophysiol* 94(3):2073–2085.
35. Beenhakker MP, Huguenard JR (2010) Astrocytes as gatekeepers of GABAB receptor function. *J Neurosci* 30(45):15262–15276.
36. Jensen K, Chiu CS, Sokolova I, Lester HA, Mody I (2003) GABA transporter-1 (GAT1)-deficient mice: Differential tonic activation of GABAA versus GABAB receptors in the hippocampus. *J Neurophysiol* 90(4):2690–2701.
37. De Biasi S, Vitellaro-Zuccarello L, Brecha NC (1998) Immunoreactivity for the GABA transporter-1 and GABA transporter-3 is restricted to astrocytes in the rat thalamus: A light and electron-microscopic immunolocalization. *Neuroscience* 83(3):815–828.
38. Vitellaro-Zuccarello L, Calvaresi N, De Biasi S (2003) Expression of GABA transporters, GAT-1 and GAT-3, in the cerebral cortex and thalamus of the rat during postnatal development. *Cell Tissue Res* 313(3):245–257.
39. Christian CA, Huguenard JR (2013) Sniffer patch laser uncaging response (SPLURgE): An assay of regional differences in allosteric receptor modulation and neurotransmitter clearance. *J Neurophysiol* 110(7):1722–1731.
40. Barres BA (2008) The mystery and magic of glia: A perspective on their roles in health and disease. *Neuron* 60(3):430–440.
41. Ward AA, Jr. (1947) Convulsive activity induced by fluoroacetate. *J Neurophysiol* 10(2):105–111.
42. Chenoweth MB, St John EF (1947) Studies on the pharmacology of fluoroacetate: Effects on the central nervous systems of dogs and rabbits. *J Pharmacol Exp Ther* 90(1):76–82.
43. Goldberg ND, Passonneau JV, Lowry OH (1966) Effects of changes in brain metabolism on the levels of citric acid cycle intermediates. *J Biol Chem* 241(17):3997–4003.
44. Hornfeldt CS, Larson AA (1990) Seizures induced by fluoroacetic acid and fluorocitric acid may involve chelation of divalent cations in the spinal cord. *Eur J Pharmacol* 179(3):307–313.
45. Bryant AS, Li B, Beenhakker MP, Huguenard JR (2009) Maintenance of thalamic epileptiform activity depends on the astrocytic glutamate-glutamine cycle. *J Neurophysiol* 102(5):2880–2888.
46. Huguenard JR, McCormick DA (2007) Thalamic synchrony and dynamic regulation of global forebrain oscillations. *Trends Neurosci* 30(7):350–356.
47. Thompson SM, Gähwiler BH (1992) Effects of the GABA uptake inhibitor tiagabine on inhibitory synaptic potentials in rat hippocampal slice cultures. *J Neurophysiol* 67(6): 1698–1701.
48. Isaacson JS, Solís JM, Nicoll RA (1993) Local and diffuse synaptic actions of GABA in the hippocampus. *Neuron* 10(2):165–175.
49. Scanziani M (2000) GABA spillover activates postsynaptic GABA(B) receptors to control rhythmic hippocampal activity. *Neuron* 25(3):673–681.
50. Nusser Z, Mody I (2002) Selective modulation of tonic and phasic inhibitions in dentate gyrus granule cells. *J Neurophysiol* 87(5):2624–2628.
51. Engel D, et al. (1998) Laminar difference in GABA uptake and GAT-1 expression in rat CA1. *J Physiol* 512(Pt 3):643–649.
52. Kang J, Jiang L, Goldman SA, Nedergaard M (1998) Astrocyte-mediated potentiation of inhibitory synaptic transmission. *Nat Neurosci* 1(8):683–692.
53. Ortinski PI, et al. (2010) Selective induction of astrocytic gliosis generates deficits in neuronal inhibition. *Nat Neurosci* 13(5):584–591.
54. Liu QY, Schaffner AE, Chang YH, Maric D, Barker JL (2000) Persistent activation of GABA(A) receptor/Cl(–) channels by astrocyte-derived GABA in cultured embryonic rat hippocampal neurons. *J Neurophysiol* 84(3):1392–1403.
55. Kozlov AS, Angulo MC, Audinat E, Charpak S (2006) Target cell-specific modulation of neuronal activity by astrocytes. *Proc Natl Acad Sci USA* 103(26):10058–10063.
56. Lee S, et al. (2010) Channel-mediated tonic GABA release from glia. *Science* 330(6005):790–796.
57. Benedetti B, Matyash V, Kettenmann H (2011) Astrocytes control GABAergic inhibition of neurons in the mouse barrel cortex. *J Physiol* 589(Pt 5):1159–1172.
58. Abrahamsen H, Stenmark H (2010) Protein secretion: Unconventional exit by exophagy. *Curr Biol* 20(9):R415–R418.
59. Duran JM, Anjard C, Stefan C, Loomis WF, Malhotra V (2010) Unconventional secretion of Acb1 is mediated by autophagosomes. *J Cell Biol* 188(4):527–536.
60. Manjithaya R, Anjard C, Loomis WF, Subramani S (2010) Unconventional secretion of *Pichia pastoris* Acb1 is dependent on GRASP protein, peroxisomal functions, and autophagosome formation. *J Cell Biol* 188(4):537–546.
61. Hamilton NB, Attwell D (2010) Do astrocytes really exocytose neurotransmitters? *Nat Rev Neurosci* 11(4):227–238.
62. Araque A, Li N, Doyle RT, Haydon PG (2000) SNARE protein-dependent glutamate release from astrocytes. *J Neurosci* 20(2):666–673.
63. Perea G, Araque A (2007) Astrocytes potentiate transmitter release at single hippocampal synapses. *Science* 317(5841):1083–1086.
64. Schubert V, Bouvier D, Volterra A (2011) SNARE protein expression in synaptic terminals and astrocytes in the adult hippocampus: A comparative analysis. *Glia* 59(10): 1472–1488.
65. Ohgami RS, et al. (2005) nm1054: A spontaneous, recessive, hypochromic, microcytic anemia mutation in the mouse. *Blood* 106(10):3625–3631.
66. Huguenard JR, Prince DA (1994) Clonazepam suppresses GABAB-mediated inhibition in thalamic relay neurons through effects in nucleus reticularis. *J Neurophysiol* 71(6): 2576–2581.

Supporting Information

Christian and Huguenard 10.1073/pnas.1318031110

SI Materials and Methods

Animals. All procedures were approved by Stanford University's Administrative Panel on Laboratory Animal Care. WT C57BL/6 (Charles River Laboratories) and α3(H126R) knock-in mutant mice (1, 2) on a C57BL/6 background were bred and housed on a 12-h:12-h light:dark photoperiod with food and water available ad libitum. Because the α3 subunit gene is located on the X chromosome, α3(H126R) mutant mice were either homozygote female or hemizygote male. Mice heterozygous for the *nm1054* mutation on the 129S6/SvEvTac background were bred to yield WT, heterozygous, and homozygous mutant pups as described previously (2, 3). Homozygotes are referred to herein as *nm1054* mice; no heterozygotes were used in this study.

Brain Slice Preparation. On postnatal day (P) 18–35, mice of either sex were anesthetized with pentobarbital sodium (55 mg/kg) injected i.p. and then decapitated. The brains were immediately removed and placed in an ice-cold (~4 °C) oxygenated [95% (vol/vol) O_2/5% (vol/vol) CO_2] sucrose slicing solution containing 234 mM sucrose, 11 mM glucose, 26 mM $NaHCO_3$, 2.5 mM KCl, 1.25 mM NaH_2PO_4, 10 mM $MgSO_4$, and 0.5 mM $CaCl_2$ (310 mOsm). Acute horizontal brain slices containing somatosensory thalamus (250 μm thickness) were prepared as described previously (4) using a Leica VT1200 microtome. Slices were incubated and continuously oxygenated in warm (~32 °C) artificial cerebrospinal fluid (ACSF) containing 10 mM glucose, 26 mM $NaHCO_3$, 2.5 mM KCl, 1.25 mM $NaHPO_4$, 1 mM $MgSO_4$, 2 mM $CaCl_2$, and 126 mM NaCl (298 mOsm) for 1 h before being transferred to room temperature (~21–23 °C). A subset of slices was treated with fluorocitrate (100 μM) for at least 30 min at room temperature before recording. Fluorocitrate stocks were prepared from DL-fluorocitric acid barium salt (Sigma-Aldrich) according to published procedures (5).

Electrophysiology. Slices were individually transferred to a recording chamber on the stage of a Zeiss Axioskop fixed-stage upright microscope continuously superfused at 2 mL/min with oxygenated ACSF at room temperature. Patch-clamp recordings were made using a MultiClamp 700A amplifier with Clampex 9.2 software (Molecular Devices), and signals were digitized using a Digidata 1322A system (Molecular Devices). Borosilicate glass recording pipettes were prepared using a model P-97 Flaming/Brown micropipette puller (Sutter Instrument) to 2–5 MΩ tip resistance when filled with pipette solution. For spontaneous inhibitory postsynaptic current (sIPSC) and sniffer patch recordings, pipettes were filled with an isotonic chloride solution containing 135 mM CsCl, 10 mM Hepes, 10 mM EGTA, 2 mM $MgCl_2$, and 5 mM QX-314, with pH adjusted to 7.3 with CsOH (290 mOsm). Access resistance (R_s), measured from the peak of the averaged current response to 65 40-ms, 5-mV depolarizing steps from a holding potential of −70 mV, was <20 MΩ in all whole-cell recordings.

For current-clamp recordings, the pipette solution contained 120 mM K-gluconate, 11 mM KCl, 1 mM $MgCl_2$, 1 mM $CaCl_2$, 10 mM Hepes, and 1 mM EGTA, with pH adjusted to 7.4 with KOH (290 mOsm). Recordings were corrected for an estimated −15 mV liquid junction potential. Kynurenic acid (1–2 mM; Abcam) was used to block ionotropic glutamate receptors, and picrotoxin (50 μM; TCI America) was used to block $GABA_A$ receptors.

Whole-cell recordings of sIPSCs were made in voltage-clamp mode with the membrane potential clamped at −60 mV. Recordings were not corrected for an estimated −5-mV liquid junction potential. Signals were recorded in gap-free mode and low-pass filtered at 2 kHz with gain set at 20 mV/pA. Ionotropic glutamate receptors were blocked with kynurenic acid (1–2 mM; Abcam).

For sniffer patch recordings, outside-out membrane patches were pulled from ventrobasal nucleus (VB) neurons and placed within thalamic reticular nucleus (nRT) or VB tissue as described previously (2). In brief, alpha-carboxy-2-nitrobenzyl ester–caged GABA (100 μM; Invitrogen) was added to a 15-mL recirculating-bath ACSF solution containing D-(-)-2-amino-5-phosphonovaleric acid (APV, 100 mM, Abcam) plus 6,7-dinitroquinoxaline-2,3-dione (DNQX, 20 mM, Abcam). UV light pulses were delivered using a laser beam (355-nm wavelength; DPSS Lasers) directed into the epifluorescence port of the microscope and through the back aperture of a 60× water immersion objective. Pulses of 1-ms duration were applied at 10-s intervals. Recordings were made in voltage-clamp mode at a −30-mV holding potential with a 20-mV/pA gain and low-pass filtered at 2 kHz.

Where indicated, the benzodiazepine-binding site antagonist flumazenil (FLZ, 1 μM; Sigma-Aldrich) and/or the GABA transporter (GAT)-1 antagonist 1,2,5,6-Tetrahydro-1-[2-[[(diphenylmethylene)amino]oxy]ethyl]-3-pyridinecarboxylic acid hydrochloride (NNC-711, 4 μM; Tocris Bioscience) and the GAT-3 antagonist 1-[2-[*Tris*(4-methoxyphenyl)methoxy]ethyl]-(*S*)-3-piperidinecarboxylic acid (SNAP-5114, 10 μM; Tocris) were included in the ACSF bath solution.

Histology and Immunocytochemistry. Mice were anesthetized with Beuthanasia-D (110 mg/kg) and perfused transcardially with saline, followed by 4% paraformaldehyde (PFA; Sigma-Aldrich) in 0.1 M phosphate buffer at pH 7.4. The brains were removed and postfixed in 4% PFA at 4 °C overnight, then cryoprotected in 30% sucrose buffer and frozen on dry ice. Horizontal 50-μm slices were cut with a sliding microtome (Microm HM 400). Free-floating sections were incubated for 1 h in 10% normal donkey serum, followed by incubation with primary antibodies against diazepam-binding inhibitor (DBI) (rabbit polyclonal, 1:50; Santa Cruz Biotechnology), GFAP (mouse monoclonal, 1:500; Sigma-Aldrich), and/or neuron-specific nuclear protein (NeuN, mouse monoclonal, 1:500; Millipore) at 4 °C for 48 h on a shaker. Sections were then rinsed in PBS and incubated for 2 h with corresponding fluorescent secondary antibodies (Jackson ImmunoResearch Laboratories). Sections were mounted on slides and coverslipped with Vectashield mounting media (Vector Laboratories).

For sulforhodamine 101 (SR101) staining (6, 7), 250-μm-thick slices were prepared as for electrophysiology, with some slices incubated in 100 μM fluorocitrate (FC) for 30 min at room temperature as described above. Slices were incubated in 1 μM SR101 (Sigma-Aldrich) in oxygenated ACSF for 20 min at 34 °C, then washed in ACSF for at least 10 min at 34 °C. The slices were fixed in 4% PFA overnight, washed in PBS, resectioned to 50-μm thickness, and processed for GFAP and NeuN immunoreactivity.

Z-stacks of images with an optical distance of 0.5 μm were captured with a laser scanning confocal microscope (Zeiss LSM 510) using a 40× oil-immersion objective. Secondary antibodies tagged to fluorescein 488 and Cy3 were excited with 488- and 594- nm lasers and observed through 510–530 and 560–615 emission filters, respectively. A pinhole of 1 Airy unit and identical settings for the detector gain and amplifier offset were used to capture all confocal images.

Data Analysis and Statistics. sIPSCs were analyzed using the custom software programs wDetecta and WinScanSelect as described previously (2, 8). An event detection threshold was confirmed for each cell and was typically set at 4–8 pA above baseline. Only those sIPSCs that decayed completely to baseline before the initiation of a subsequent event and did not initiate during the decay phase of a previous event were included in kinetics analyses. All sIPSCs were used in frequency analyses. Uncaged recordings were analyzed using Clampfit 9.2 (Molecular Devices).

Voltage–current (V–I) plots were constructed from a series of current steps in 20-pA increments from −140 to 140 pA from a holding potential of −75 mV. Owing to the deinactivation and strong contribution of low-threshold Ca^{2+} bursts to firing in nRT cells (9), action potential frequency was measured during the last 100 ms of the 750-ms square pulse depolarization and used to calculate the frequency–current (F–I) curve slope. The rheobase (i.e., minimal current required to trigger action potential firing) was also calculated from these depolarizing steps. The input resistance (R_{in}) and membrane time constant (τ_m) were measured from the linear portion of the V–I plot. Resting membrane potential was measured from the baseline portion of a voltage response recorded with no injected holding current at ∼1 min after the whole-cell configuration was achieved. Capacitance was measured in voltage-clamp mode from the integral of the averaged current response to 65 40-ms, 5-mV depolarizing steps from a holding potential of −70 mV.

Data were transferred to Excel (Microsoft), Origin 7 (Microcal Software), and SigmaStat (Aspire Software) for statistical analysis. Comparisons between groups were performed using one-way ANOVA, two-tailed independent or paired *t* tests, or the nonparametric Mann–Whitney rank-sum test. Cumulative probability distributions were constructed using up to 100 randomly selected sIPSCs per cell and compared using two-sample Kolmogorov–Smirnov goodness-of-fit tests. Data are presented as mean ± SEM. Statistical significance was set at $P < 0.05$ for mean value comparisons and at $P < 0.001$ for Kolmogorov–Smirnov tests.

1. Löw K, et al. (2000) Molecular and neuronal substrate for the selective attenuation of anxiety. *Science* 290(5489):131–134.
2. Christian CA, et al. (2013) Endogenous positive allosteric modulation of GABA(A) receptors by diazepam binding inhibitor. *Neuron* 78(6):1063–1074.
3. Ohgami RS, et al. (2005) nm1054: A spontaneous, recessive, hypochromic, microcytic anemia mutation in the mouse. *Blood* 106(10):3625–3631.
4. Huguenard JR, Prince DA (1994) Clonazepam suppresses GABAB-mediated inhibition in thalamic relay neurons through effects in nucleus reticularis. *J Neurophysiol* 71(6): 2576–2581.
5. Paulsen RE, Contestabile A, Villani L, Fonnum F (1987) An in vivo model for studying function of brain tissue temporarily devoid of glial cell metabolism: The use of fluorocitrate. *J Neurochem* 48(5):1377–1385.
6. Kafitz KW, Meier SD, Stephan J, Rose CR (2008) Developmental profile and properties of sulforhodamine 101–labeled glial cells in acute brain slices of rat hippocampus. *J Neurosci Methods* 169(1):84–92.
7. Nimmerjahn A, Kirchhoff F, Kerr JN, Helmchen F (2004) Sulforhodamine 101 as a specific marker of astroglia in the neocortex in vivo. *Nat Methods* 1(1):31–37.
8. Huntsman MM, Porcello DM, Homanics GE, DeLorey TM, Huguenard JR (1999) Reciprocal inhibitory connections and network synchrony in the mammalian thalamus. *Science* 283(5401):541–543.
9. Huguenard JR, Prince DA (1992) A novel T-type current underlies prolonged Ca(2+)-dependent burst firing in GABAergic neurons of rat thalamic reticular nucleus. *J Neurosci* 12(10):3804–3817.

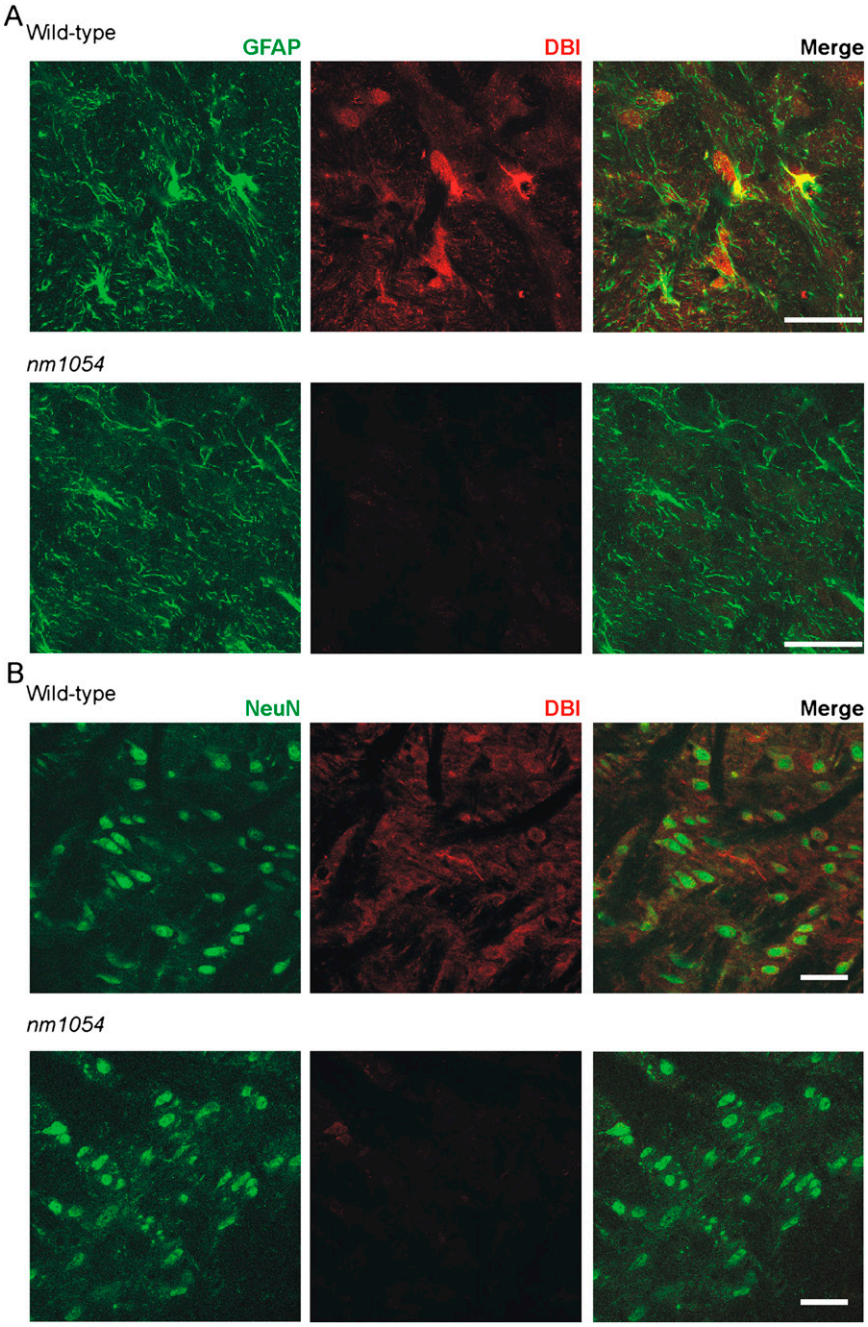

Fig. S1. DBI immunoreactivity colocalizes with astrocytic and neuronal markers in the nRT of WT mice, but not in that of *nm1054* mutants. (*A*) Fluorescence images of immunostaining for DBI (red) and the astrocytic marker GFAP (green) in a WT mouse (*Upper*) and an *nm1054* mutant mouse (*Lower*). (*B*) Fluorescence images of immunostaining for DBI (red) and the neuronal marker NeuN (green) in a WT mouse (*Upper*) and an *nm1054* mutant mouse (*Lower*). (Scale bars: 20 μm in *A*; 40 μm in *B*.)

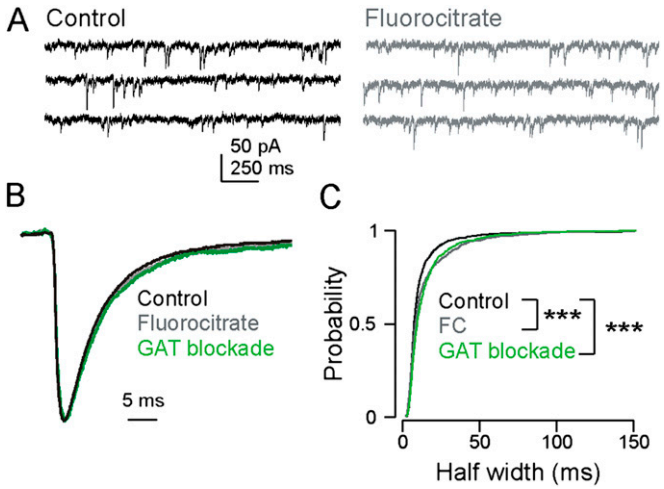

Fig. S2. FC increases sIPSC duration in VB neurons via reductions in GAT activity. (*A*) Representative continuous sIPSC traces recorded in VB cells from C57BL/6 mice under control conditions (black traces) and after FC treatment (gray traces). (*B*) Averaged sIPSCs from VB cells under control conditions (black trace), after FC treatment (gray trace), and under GAT blockade conditions (green trace), normalized to peak amplitude. (*C*) Probability distributions comparing sIPSC half-width under control (black trace), FC-treated (gray trace), and GAT blockade (GAT, green trace) conditions (n = 800–1,400 events/group). ***$P < 0.001$ vs. control.

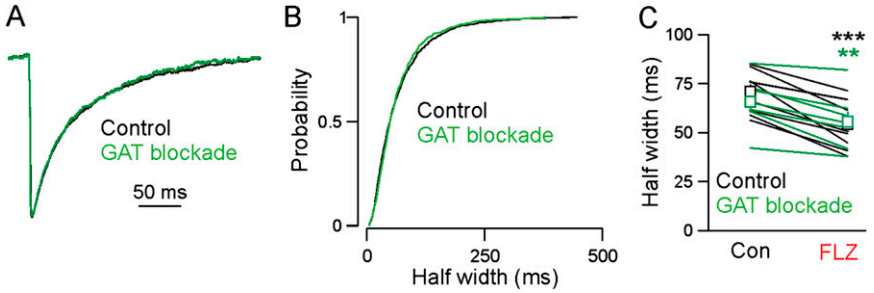

Fig. S3. GAT blockade alone does not alter sIPSC duration or response to FLZ in the nRT. (*A*) Averaged sIPSCs from nRT cells under control conditions (black trace) and after GAT blockade treatment (green trace), normalized to peak amplitude. (*B*) Probability distributions comparing sIPSC half-width under control (black trace) and GAT blockade (green trace) conditions (n = 1,000–1,200 events/group). (*C*) sIPSC half-width in nRT cells before (Con) and during FLZ treatment under control (n = 9 cells; black lines) and GAT blockade conditions (n = 7 cells; green lines). Open boxes indicate mean ± SEM. **$P < 0.01$; ***$P < 0.001$ vs. control.

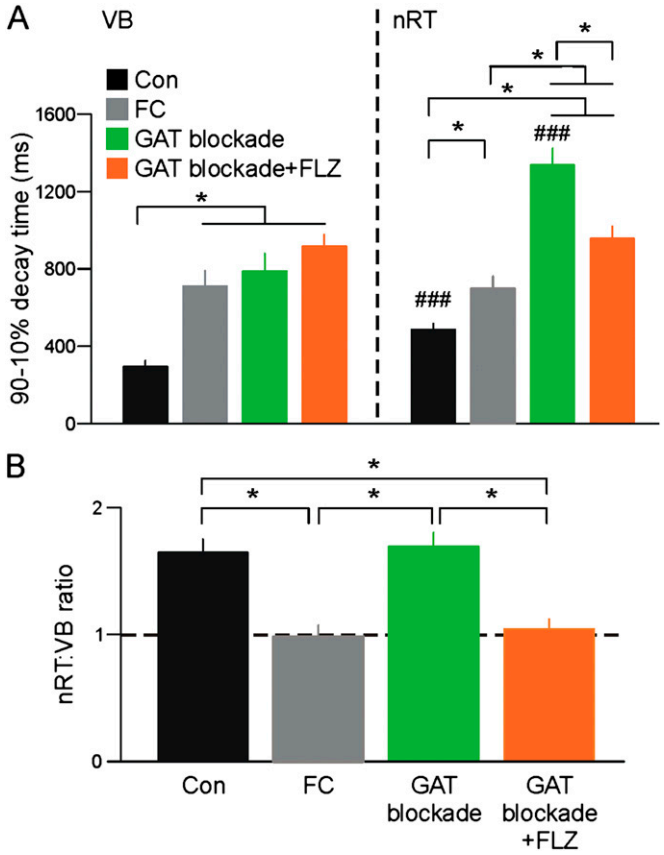

Fig. S4. Late decay properties of sniffer patch laser uncaging responses (SPLURgEs) are affected similarly by fluorocitrate and GAT blockade. (*A*) Mean ± SEM for 90–10% decay time of uncaging responses recorded under control conditions (black bars), after FC treatment (gray bars), in the presence of GAT antagonists (green bars), or in the presence of GAT antagonists and FLZ (orange bars). Each bar represents between six and nine patches. (*B*) Mean ± SEM for ratio of values obtained with patches placed in the nRT compared with patches placed in the VB for each respective group. $^{*}P < 0.05$; $^{\#\#\#}P < 0.001$ vs. respective group values for patches placed in VB.

Table S1. Intrinsic membrane and firing properties of nRT neurons are not affected by FC treatment

	R_{in}, MΩ	RMP, mV	τ_m, ms	AP threshold, mV	Rheobase, pA	*F-I* slope, Hz/pA
Control	284.11 ± 21.37	−68.36 ± 1.71	28.09 ± 3.25	−49.68 ± 2.02	50.91 ± 6.80	0.31 ± 0.14
FC-treated	372.70 ± 61.60	−68.22 ± 3.53	37.24 ± 7.08	−52.16 ± 2.67	44.00 ± 11.85	0.39 ± 0.12
P value	0.17	0.97	0.24	0.46	0.61	0.69

Values are calculated from WT C57BL/6 nRT neurons in control conditions ($n = 11$) and after FC treatment ($n = 10$). R_{in}, *F-I* slope, τ_m, AP threshold, and rheobase were calculated from cells held at a membrane potential of −75 mV in current-clamp mode. RMP was calculated from traces in which no current was injected. All values are expressed as mean ± SEM. R_{in}, input resistance; RMP, resting membrane potential; *F-I* slope, frequency-current slope; τ_m, membrane time constant; AP, action potential.